

# Macrophage Plasticity is Rac Signalling and MMP9 Dependant

**Jana Travnickova**

LIPH, CNRS, INSERM, Univ Montpellier, Montpellier, France - Emergence of haematopoietic stem cells and cancer

**Sandra Nhim**

LIPH, CNRS, INSERM, Univ Montpellier, Montpellier, France - Emergence of haematopoietic stem cells and cancer

**Naoill Abdellaoui**

LIPH, CNRS, INSERM, Univ Montpellier, Montpellier, France - Emergence of haematopoietic stem cells and cancer

**Farida Djouad**

IRMB, Inserm U1183, CHU Saint Eloi- Cellules souches, Blastème et Régénération, F-34295, Montpellier

**Mai Nguyen-Chi**

LIPH, CNRS, INSERM, Univ Montpellier, Montpellier, France - Mise en place de l'immunité et inflammation

**Andrea Parmeggiani**

Laboratoire Charles Coulomb, CNRS, Univ Montpellier, UMR 5221 - CNRS/UM Complex Systems and Non Linear Phenomena

**Karima Kissa** (✉ [karima.kissa-marin@umontpellier.fr](mailto:karima.kissa-marin@umontpellier.fr))

LIPH, CNRS, INSERM, Univ Montpellier, Montpellier, France - Emergence of haematopoietic stem cells and cancer

---

## Research Article

**Keywords:** ECM, MMPs, HSPCs

**Posted Date:** November 30th, 2020

**DOI:** <https://doi.org/10.21203/rs.3.rs-109336/v1>

**License:**  This work is licensed under a Creative Commons Attribution 4.0 International License.

[Read Full License](#)

---

# Macrophage plasticity is Rac signalling and MMP9 dependant

---

Jana Travnickova<sup>1</sup>, Sandra Nhim<sup>1</sup>, Naoill Abdellaoui<sup>1</sup>, Farida Djouad<sup>2</sup>, Maï Nguyen-Chi<sup>3</sup>, Andrea Parmeggiani<sup>1,4</sup> and Karima Kissa<sup>1,\*</sup>

<sup>1</sup> LIPH, CNRS, INSERM, Univ Montpellier, Montpellier, France - Emergence of haematopoietic stem cells and cancer

<sup>2</sup> IRMB, Inserm U1183, CHU Saint Eloi- Cellules souches, Blastème et Régénération, F-34295, Montpellier, France

<sup>3</sup> LIPH, CNRS, INSERM, Univ Montpellier, Montpellier, France - Mise en place de l'immunité et inflammation

<sup>4</sup> Laboratoire Charles Coulomb, CNRS, Univ Montpellier, Montpellier, France

\*Correspondence: karima.kissa-marin@umontpellier.fr

**26 402 characters including spaces**

17 **Abstract**

18 *In vitro*, depending on extracellular matrix (ECM) architecture, macrophages migrate  
19 either in amoeboid or mesenchymal mode; while the first is a general trait of leukocytes, the latter  
20 is associated with tissue remodelling via Matrix Metalloproteinases (MMPs). To assess whether  
21 these stereotyped migrations could be also observed in a physiological context, we used the  
22 zebrafish embryo and monitored macrophage morphology, behaviour and capacity to  
23 mobilisation haematopoietic stem/progenitor cells (HSPCs), as a final functional readout.  
24 Morphometric analysis identified 4 different cell shapes. Live imaging revealed that macrophages  
25 successively adopt all four shapes as they migrate through ECM. Treatment with inhibitors of  
26 MMPs or Rac GTPase to abolish mesenchymal migration, suppresses both ECM degradation and  
27 HSPC mobilisation while differently affecting macrophage behaviour. This study depicts real  
28 time macrophage behaviour in a physiological context and reveals extreme reactivity of these  
29 cells constantly adapting and switching migratory shapes to achieve HSPCs proper mobilisation.

30

## 31 **Introduction**

32 Macrophages were for the first time identified as phagocytic cells responsible for pathogen  
33 elimination (Metchnikoff, 1892). Over the past century, they were associated with homeostasis,  
34 innate and adaptive immune responses, inflammation, tissue remodelling and cytokine production  
35 (Gordon and Taylor, 2005; Wynn et al., 2013). Macrophages are the most plastic haematopoietic  
36 cells present in all tissues; their diversity depends upon their location, their morphology, their  
37 membrane receptors or surface markers (Wynn et al., 2013). Depending on tissue composition  
38 they infiltrate and environmental constraints, macrophages adopt different migration modes  
39 (Vérollet et al., 2011). In the course of a three-dimensional (3D) migration, macrophages can  
40 either adopt an amoeboid or a mesenchymal migratory mode. In case of an amoeboid migration,  
41 cells take on a round or polarised shape and migrate through the extracellular matrix (ECM).  
42 Such a migration is Rho/Rock GTPases dependent. During mesenchymal migration,  
43 macrophages degrade the ECM through proteinases secretions (e.g. Matrix Metalloproteinases or  
44 MMPs) and cells take on an elongated shape. This second migratory mode is Rac GTPase  
45 signalling dependent (Sanz-Moreno and Marshall, 2010; Vérollet et al., 2011).

46 In mouse and human, macrophage characterization was mainly performed *in vitro* using bone  
47 marrow derived macrophages. Recently, the zebrafish model was used to resolve specific issues  
48 during the developmental process or to address accurate pathologies. The transparency of  
49 zebrafish embryos enables the live imaging and real time tracking of cell populations. We and  
50 other groups have shown that two main waves of macrophages emerge from primitive and  
51 definitive haematopoiesis during the zebrafish development (Gering and Patient, 2005; Herbomel  
52 et al., 1999; Murayama et al., 2006). The initial wave takes place between 18 and 25 hours post  
53 fertilization (hpf) in the yolk sac (Herbomel et al., 1999). The second wave occurs between 30  
54 and 55 hpf in the aorta-gonad-mesonephros (AGM) (Gering and Patient, 2005; Murayama et al.,

55 2006) and generates the haematopoietic stem/progenitor cells (HSPCs) (Bertrand et al., 2010;  
56 Kissa and Herbomel, 2010) which later will differentiate into all blood cells including  
57 macrophages. Finally, a transient hematopoietic wave is initiated in the posterior blood island,  
58 giving rise to the multilineage progenitor cells and erythromyeloid progenitors, which develop  
59 into both erythroid and myeloid cells (Bertrand et al., 2007).

60 Recently, we demonstrated *in vivo* that primitive macrophages are crucial in the establishment of  
61 a definitive haematopoiesis (Travnickova et al., 2015). Macrophages that accumulated in the  
62 AGM degrade the ECM located in the vicinity of HSPCs via matrix metalloproteinase 9 (MMP-9)  
63 secretions, thereby enabling them to migrate, enter the blood stream and colonise haematopoietic  
64 organs.

65 In the present study, we provide an extensive analysis of macrophages in zebrafish embryos.  
66 Using morphological analysis we were able to distinguish for the first time different macrophage  
67 subtypes *in vivo*. By combining morphological analysis with live imaging we succeeded in  
68 visualizing the dynamic behavioural patterns of individual macrophages during their migration  
69 through the ECM.

70

71

## 72 **Results**

### 73 **Macrophage shape heterogeneity in the zebrafish embryo**

74 During the establishment of the definitive haematopoiesis, macrophages accumulated in the  
75 AGM between 30 and 60 hpf degrade the ECM surrounding HSPCs via Mmp-9 secretions which  
76 result in the mobilization of HSPCs (Travnickova et al., 2015). Using this physiological model,  
77 we analysed the shape and behaviour of proteolytic macrophage in order to establish a potential  
78 correlation. We first described the position and shape of macrophages in the AGM using the  
79 *kdrl:eGFP//mpeg1:mCherry-F* double transgenic lines where the GFP protein highlighted vessels  
80 and mCherry-F macrophage membranes (**Fig. 1A-B**). Figure 1A provides a schematic view of the  
81 vessel and macrophage position as shown in Figure 1B. Using a 3D view (**Fig. 1B**) we were able  
82 to determine the position of macrophages (white arrows) in the outer layer of the vein wall  
83 between the vein and the aorta floor with different morphologies. The particle analysis of  
84 macrophages from a maximum projected confocal acquisitions enabled us to distinguish and  
85 quantify the various macrophage shapes. Three main morphological criteria were identified:  
86 circularity, roundness and elongation factor (**Fig. 1C and Suppl. Table 1**). They revealed the  
87 existence of 4 main shapes whose images are shown in **Figure 1D**. We named these 4 subgroups  
88 - round (1), amoeboid (2), star-like (3) and elongated shape (4). While the round and elongated  
89 shapes had already been described *in vitro*, the two remaining shapes might represent either  
90 subgroups present *in vivo* or intermediate stages between round and elongated shapes. The main  
91 difference between the amoeboid and star-like shapes lied in the presence in the amoeboid shape  
92 of a main axis, i.e. polarity. The quantification of each shape revealed that amoeboid, star-like  
93 and elongated shapes were equally present whereas the round shape remained sparse (**Fig. 1E**).

94

95 **Dynamics of macrophage migration *in vivo***

96 The analysis of macrophage shapes revealed the existence of four morphological subgroups  
97 distributed in the zebrafish AGM. To assess the behaviour of each macrophage subgroup, we  
98 imaged *Tg(Mpeg1:mCherry)* embryos over the course of one hour (acquisition every minute;  
99 **Video 1**). We selected time frames in colour depth projection that illustrated the dynamics of  
100 macrophages able to adopt different shapes within fifteen minutes (**Fig. 2A-F and Video 1**,  
101 colour code scale). The outlines represent the shape of macrophages in the imaged area at the 9th  
102 minute and enable us to draw a direct comparison with following time points. The colour depth  
103 projection of confocal imaging enabled us to determine the depth of macrophage positions *in vivo*  
104 and to demonstrate their ability to migrate in 3D patterns (**Video 1**). *In vivo* tracking of all  
105 macrophages within a 60 minute timeframe demonstrated that no specific directionality was  
106 maintained during their migration (**Fig. 2G**, n=23) as opposed to macrophages attracted to a  
107 wound site as an example of typical oriented migration (**Fig. 2H**, n=27). The speed of migration  
108 remained the same in both cases (data not shown). Subsequently, we quantified the evolution of  
109 macrophage shapes over time. Every single macrophage in the AGM reveals an ability to change  
110 shape within a very short time span (measured every 5 minutes) and to pass repeatedly through  
111 distinct shape subgroups over a 30 minutes course (**Fig. 2I**, n=10). The round shape appeared less  
112 frequently than others and live imaging showed that cells often adopted a round shape under two  
113 specific conditions: during cell division or once the macrophage entered the bloodstream.  
114 In conclusion, macrophage real time imaging completes the characterisation of mesenchymal  
115 migrating macrophages and shows for the first time that they can adopt successive morphologies  
116 for their migration in the 3D matrix.

117

118

## 119 **Rac inhibition modifies macrophage behaviour and function**

120 Using *in vivo* imaging we showed that macrophages exhibited morphological plasticity during  
121 their migration. This high plasticity depended on both, external (the stroma rigidity) and intrinsic  
122 parameters (cytoskeleton dynamics) (Vérollet et al., 2011). One intrinsic factor associated with  
123 mesenchymal migration is the small GTPase- Rac signalling. We thus investigated the effect of  
124 Rac chemical inhibition on macrophage shape and migration patterns. The macrophage shape  
125 distribution in Rac inhibitor (NSC23766) treated embryos did not significantly differ from that of  
126 DMSO treated control (**Fig. 3A**,  $N_{\text{DMSO}}=10$  and  $N_{\text{Rac inh.}}=15$  embryos). Selected images from  
127 **Video 2** (colour, depth, projection, bottom) demonstrated that the macrophage migration was  
128 much slower than that of control embryos (**Fig. 3B-E, Video 2**, top). Macrophage speed  
129 measured over 60 minutes in the AGM confirmed a decrease in velocity from  $2.37 \pm 0.13$   
130  $\mu\text{m}\cdot\text{min}^{-1}$  to  $1.13 \pm 0.16 \mu\text{m}\cdot\text{min}^{-1}$  (**Fig. 3F**).

131 The tracking plot diagram illustrated macrophage migration path and distance in control and Rac-  
132 inhibited embryos (**Fig. 3G-H**,  $n=15$  macrophages from 4 embryos, position measured every  
133 minute over 1 hour) and revealed that Rac inhibition reduced macrophage moves from  $130.9 \pm 7.5$   
134  $\mu\text{m}$  to  $56.8 \pm 7.8 \mu\text{m}$ . Moreover, the analysis of macrophage shape dynamics, revealed a  
135 reduction in macrophage plasticity over time as macrophages were no longer able to  
136 consecutively adopt different shapes (**Fig. 3I, right**;  $n= 7$ ) versus control (**Fig. 3I, left**;  $n= 7$ ).  
137 However, in spite of reduced plasticity levels, membrane extensions were still formed at the same  
138 rate and with similar length as in control macrophages. Rac inhibition resulted in an increase in  
139 single extension span (from  $2.8 \pm 0.3 \text{ min}$  to  $11.0 \pm 1.9 \text{ min}$ ,  $n_{\text{extension}}= 45$ ) as opposed to that of  
140 control macrophages.

141 As macrophage migration and morphological plasticity were significantly affected by Rac  
142 inhibition, we decided to evaluate the functionality of these macrophages. The main role of AGM

143 macrophages is to degrade the ECM and to enable HSPC migration (Travnickova et al., 2015). *In*  
144 *vivo* zymography of *Tg(Mpeg1:mCherry)* embryos at 48 hpf, revealed a significant reduction in  
145 gelatin degradation and thereby a lower gelatinase activity (decreased number of green dots of  
146 cleavage-revealed FITC) in Rac inhibited embryo compared to control (**Fig. 3J**). Since the  
147 proteolytic function of macrophages in the AGM is essential to HSPC mobilisation, we assessed  
148 the effect of Rac inhibition on haematopoietic organ colonisation. We noticed an increase in  
149 HSPCs accumulated in the AGM at 48 hpf ( $+70\pm 8\%$ , n=6) and consequently a decrease in HSPC  
150 accumulated in the CHT at 55 hpf ( $-41\pm 2\%$ ; n=5).

151

152

### 153 **MMP inhibition affects macrophage shape, behaviour and function.**

154 Rac inhibition has an impact on macrophage proteolytic activity and consequently on their  
155 function. To assess whether direct inhibition of macrophage proteolytic activity induces a similar  
156 behaviour, we soaked embryos in a medium containing SB-3CT MMP inhibitor. We previously  
157 demonstrated that ECM degradation occurred as a result of macrophage-secreted MMP-9 around  
158 HSPCs to enable their intravasation. We evaluated the direct impact of MMP inhibition on  
159 macrophage morphology and noticed a variation in shape distribution: an increase in round shape  
160 number and a decrease in star-like and elongated shapes (**Fig. 4A**). Moreover, MMP inhibition  
161 affected macrophage migration and behaviour (**Fig. 4B-E, Video 3**). Selected images from **Video**  
162 **3** displayed a typical example of macrophage migration pattern. Using Colour depth projection  
163 we were able to visualise the 3D migration of macrophages in the AGM and noticed that in  
164 MMP-9 inhibited embryos, macrophages migrated mainly in 2D. At a given point in time, they  
165 adopted a single colour whereas in control embryos we observed dynamic changes indicated by  
166 the presence of several colours at one time point (**Fig. 2A-F**). Moreover, **Video 3** showed the

167 macrophages adopted different migration pattern resembling to the leukocyte crawling on vein  
168 vessel.

169 Furthermore, we observed that MMP inhibition affected macrophage velocity and directionality.

170 The speed of migration increased more than 3 times compared to the control (from  $2.20 \pm 0.11$

171  $\mu\text{m}\cdot\text{min}^{-1}$  to  $7.80 \pm 0.92 \mu\text{m}\cdot\text{min}^{-1}$ ; **Fig. 4F**). Finally, a tracking plot diagram which illustrated the

172 migration path and distance of macrophages in the AGM in control and MMP-inhibited embryos

173 (**Fig. 4G and H**) revealed that migration directionality increased from 0.27 to 0.66. Cell tracking

174 showed that macrophages migrated along the vein, in the same direction as the blood flow. We

175 concluded that, MMP inhibition affected both macrophage shape and migration patterns. They

176 adopted a MMP independent migration pattern with increased velocity which was reminiscent of

177 an amoeboid type of migration.

178

179

180

## 181 **Discussion**

182 In this study we characterised in zebrafish embryos the macrophage population present in the  
183 AGM with a known proteolytic function (Travnickova et al., 2015). We reported the existence of  
184 four macrophage morphological subgroups. Previous studies performed *in vitro* described two  
185 major morphological types, elongated and rounded shapes (McWhorter et al., 2013). Using *in*  
186 *vivo* analyses we were able to identify two additional morphological shapes: amoeboid and star-  
187 like shapes. *In vivo* observations revealed the presence of a higher number of macrophage  
188 subgroups in contrast to conclusions drawn from assays on 3D matrices, thereby suggesting the  
189 importance of *in vivo* modelling to complete results obtained *in vitro*. Using high resolution live  
190 imaging in conjunction with macrophage shape descriptor analysis we devised a novel tool that  
191 enabled to quantify *in vivo* the dynamics and morphological plasticity of macrophages.

192 While macrophages were thought to exclusively migrate using an amoeboid mode (Friedl and  
193 Weigelin, 2008), Dr Parini's group demonstrated their capacity to also use a mesenchymal  
194 migration mode (Cougoule et al., 2012). In line with this last study, we describe the mesenchymal  
195 macrophage migration process *in vivo* in zebrafish embryos. Macrophages revealed an increase in  
196 shape plasticity which confirmed the outcome of previous studies performed *in vitro* (Cougoule  
197 et al., 2012).

198 Previous studies highlighted the significance of the role played by Rac signalling in cytoskeleton  
199 organisation during the mesenchymal migration of cells (Sanz-Moreno and Marshall, 2010). Our  
200 study performed *in vivo* during the establishment of haematopoiesis in zebrafish embryos also  
201 demonstrated that the mesenchymal migration of macrophages was Rac signalling dependent.  
202 Going further, we observed that Rac signalling inhibition affected not only macrophage migration  
203 but also their proteolytic function and their phenotype. Indeed, upon Rac inhibition macrophages

204 lose their ability to degrade the ECM matrix. We also observed that this treatment significantly  
205 reduced macrophage velocity and morphological plasticity. Moreover, live imaging revealed that  
206 macrophages develop and keep longer membrane extensions and that they remained longer in a  
207 specific location. Our study confirmed previous *in vitro* observations showing that Rac1-/  
208 macrophages cultured on plastic exhibited additional membrane extensions when compared to  
209 control macrophages (Wheeler et al., 2006).

210 We finally observed that the inhibition of the macrophage proteolytic function induces their  
211 transition into a different type of migration mode corresponding to the adaptation of macrophages  
212 to their new environment. They adopted a round shape with an amoeboid migration.  
213 Macrophages were no longer able to migrate within the AGM stroma and they moved along the  
214 vein wall.

215 Proteolytic macrophages in the AGM exhibited a high functional similarity to macrophages  
216 found in solid tumours referred to as tumour associated macrophages (TAM). TAM play a  
217 significant part in ECM remodelling through proteinase releases (mainly MMP-2 and 9) and  
218 allow tumour cells to join the bloodstream and to seed in secondary sites (Condeelis and Pollard,  
219 2006). Therefore, a current strategy is to target TAM to combat cancer (Panni et al., 2013).  
220 Several approaches based on macrophage depletion (clodronate liposomes) or functional  
221 modification (broad spectrum MMP inhibitors) did not succeed and failed during clinical trials  
222 due to low specificity and the amount of side effects (Panni et al., 2013; Turk, 2006). Expanding  
223 our knowledge from a purely molecular standpoint toward an in-depth understanding of  
224 behaviour and requirements in migration and site infiltration using adapted *in vivo* models, would  
225 complement existing studies and enable us to develop more targeted immunotherapeutic solutions.  
226

## 227 **Materials and Methods**

### 228 **Zebrafish husbandry**

229 Wild-type and transgenic lines were maintained in compliance with the Institutional Animal Care  
230 and Use protocols. The following transgenic lines were used in this study: *Tg(Mpeg1:mCherry-F)*  
231 (Ellett et al., 2011; Travnickova et al., 2015) for macrophage membrane marking and  
232 *Tg(kdrl:eGFP)* (Beis et al., 2005) for vessel endothelium labelling. Embryos were kept in the  
233 presence of 1-phenyl-2-thiourea to prevent melanin pigmentation (Westerfield, 2000) and staged  
234 as described by Kimmel et al (Kimmel et al., 1995). All experiments were performed in  
235 accordance with the protocol CEEA-LR-13007 approved by the Animal Care and Use  
236 Languedoc-Roussillon Committee.

237

### 238 **Live Imaging**

239 Zebrafish embryos (lateral views, rostral to the left) were embedded in 0.7% low melting agarose  
240 and imaged using a Zeiss LSM510 confocal microscope through a 40x water immersion objective  
241 with a 1024x256 pixel resolution at 28°C. All live imaging experiments were performed at 46-48  
242 hpf and all time-lapse imaging occurred at an acquisition rate of one minute at a 1µm z-interval.  
243 The acquisitions were performed using ZEN2009. Image processing such as maximum intensity  
244 projections, 3D view, and overall image contrast adjustment were performed using Fiji software.

245

### 246 **Inhibitor treatment**

247 Embryos were soaked in MMP-2 and 9 inhibitors SB-3CT (Enzo Life Sciences) 9 µM or  
248 NSC23766 Rac inhibitor (Tocris) 50 µM or DMSO 0.25% as a control from 5-prim stage (25 hpf)  
249 to 46-48 hpf. For stock solution, inhibitors were dissolved in DMSO at a 10mM concentration

250 and stored at -20°C.

251

## 252 **Image processing and macrophage shape analysis**

253 Confocal stacks of membrane-labelled macrophages were projected using a maximum intensity  
254 projection and 2D images were binarised using an automatic threshold. The following shape  
255 descriptors were evaluated using the Fiji plugin Particle analysis: area ( $\mu\text{m}^2$ ), perimeter ( $\mu\text{m}$ ),  
256 circularity and roundness. The elongation factor was manually measured by dividing the longest  
257 axis of the object by its longest perpendicular axis ( $x/y$ ). Objects with an area under  $80 \mu\text{m}^2$  were  
258 excluded from the further analysis. Circularity was calculated using the following formula:  $4\pi \times$   
259  $(\text{area}/\text{perimeter}^2)$ . This parameter varied from 0 (linear polygon) to 1 (perfect circle). Circularity  
260 was used to set apart round objects (circularity  $> 0.2$ ) and roundness and elongation factor  
261 enabled us to break down non-round subjects into 3 subgroups: elongated, amoeboid and star-like  
262 shaped. Roundness was calculated using the following formula:  $4 \times \{\text{area}/ [\pi \times (\text{major axis})^2]\}$   
263 and varied from 0 (linear polygon) to 1 (perfect round). Supplementary table 1 shows the mean  
264 values of circularity, roundness and elongation factor measured for each of the above listed  
265 subgroups.

266

## 267 **Cell tracking and velocity measurement**

268 Maximum intensity projections of 60 minute time-lapses acquired every minute were analysed  
269 using a manual tracking plugin in Fiji. Measured data were transferred into a Chemotaxis and  
270 Migration tool programme (Ibidi) to design tracking and rose plots (Figure 2G-H for rose plots,  
271 3G-H and 4G-H for tracking plots). A rose diagram maps single counts of the position of every  
272 macrophage in a selected area (black and grey sectors of angle  $\pi/18$ ) every minute over 60  
273 minutes with an  $(x,y 0,0)$  starting point. The tracking plot diagram represents the migration path

274 and distance of macrophages in the AGM with an x,y 0,0 starting point, being measured every  
275 minute over 60 minutes. The average of single macrophage velocities ( $\mu\text{m min}^{-1}$ ) during 15-60  
276 minutes were used for analysis. The evaluation of the directionality was performed using a  
277 Rayleigh statistical test for the uniformity of a circular distribution of points (end points of single  
278 macrophages). All analyses were conducted using the Chemotaxis and Migration tool software  
279 (Ibidi).

280

### 281 **Fin amputation for oriented migration analysis**

282 Caudal fin amputation was performed with a sterile scalpel at 44 hpf, posterior to muscle and  
283 notochord under anaesthesia with 0.016% Tricaine (ethyl 3-aminobenzoate, Sigma Aldrich). 4 h  
284 post amputation embryos were mounted and imaged as described above.

285

### 286 ***In vivo* zymography**

287 The *In vivo* zymography was performed according to Crawford's protocol (Crawford and Pilgrim,  
288 2005). A working solution, 1 mg ml<sup>-1</sup> of fluoresceinated gelatin (Gelatin-FITC, Anaspec) in PBS  
289 was injected (4-5 ng) into muscles between 4<sup>th</sup> and 5<sup>th</sup> somite at 42 hpf. Imaging was performed  
290 following the injections. Embryos were incubated in DMSO or Rac inhibitor from 25 hpf up to  
291 the Gelatin-FITC injections.

292

### 293 **Statistical analysis**

294 Normal distributions were analysed using the Shapiro-Wilk test. Non-Gaussian data were  
295 analysed using the Wilcoxon test, Gaussian with Student t-test. P<0.05 was considered as  
296 statistically significant (symbols: \*\*\*\*p<0.0001 \*\*\* p<0.001; \*\* p<0.01; \* p<0.05) Statistical  
297 analyses were performed using the R software.

298

## 299 **Acknowledgements**

300 We would like to thank E. Lelièvre and M. Rossel for their critical review of this manuscript; V.  
301 Diakou and the MRI facility for their assistance, A. Sahuquet for his help in the particle analysis.  
302 This work was supported by grants from the ARC, Chercheur d'Avenir - Région Languedoc-  
303 Roussillon, FRM and ATIP-Avenir. J.T. was supported by a fellowship from the MESR and  
304 FRM (FDT20150532507), NA by a fellowship from the FRM, M.N.-C. by a fellowship from the  
305 Université de Montpellier.

306

307

## 308 **Author contributions**

309 J.T., and K.K. designed the project and the experiments, J.T., S.N., M.N.-C and N.A. performed  
310 the experiments and analysed the results. J.T. and K.K. wrote the manuscript with the input of  
311 S.N., M.N.-C., F.D. and A.P.

312

## 313 **Ethics**

314 All animal experiments described in the present study were conducted at the University of  
315 Montpellier in compliance with European Union guidelines for handling of laboratory animals  
316 ([http://ec.europa.eu/environment/chemicals/lab\\_animals/home\\_en.htm](http://ec.europa.eu/environment/chemicals/lab_animals/home_en.htm)) and were approved by the  
317 Direction Sanitaire et Vétérinaire de l'Hérault and Comité d'Ethique pour l'Experimentation  
318 Animale under reference CEEA-LR-13007.

319

320

321 **Disclosure of Conflicts of Interest**

322 The authors declare no competing financial interests.

323

324 **Abbreviations**

325 AGM, Aorta-Gonad-Mesonephros

326 HSPC, Haematopoietic stem and progenitor cells

327 MMP, Matrix metalloproteinases

328 TAM, Tumour associated macrophages

## 329 **References**

- 330 Beis, D., Bartman, T., Jin, S.-W., Scott, I.C., D'Amico, L. a, Ober, E. a, Verkade, H., Frantsve, J.,  
331 Field, H. a, Wehman, A., et al. (2005). Genetic and cellular analyses of zebrafish atrioventricular  
332 cushion and valve development. *Development* *132*, 4193–4204.
- 333 Bertrand, J.Y., Kim, A.D., Violette, E.P., Stachura, D.L., Cisson, J.L., and Traver, D. (2007).  
334 Definitive hematopoiesis initiates through a committed erythromyeloid progenitor in the  
335 zebrafish embryo. *Development* *134*, 4147–4156.
- 336 Bertrand, J.Y., Chi, N.C., Santoso, B., Teng, S., Stainier, D.Y.R., and Traver, D. (2010).  
337 Haematopoietic stem cells derive directly from aortic endothelium during development. *Nature*  
338 *464*, 108–111.
- 339 Condeelis, J., and Pollard, J.W. (2006). Macrophages: obligate partners for tumor cell migration,  
340 invasion, and metastasis. *Cell* *124*, 263–266.
- 341 Cougoule, C., Van Goethem, E., Le Cabec, V., Lafouresse, F., Dupré, L., Mehraj, V., Mège, J.-L.,  
342 Lastrucci, C., and Maridonneau-Parini, I. (2012). Blood leukocytes and macrophages of various  
343 phenotypes have distinct abilities to form podosomes and to migrate in 3D environments. *Eur. J.*  
344 *Cell Biol.* *91*, 938–949.
- 345 Crawford, B.D., and Pilgrim, D.B. (2005). Ontogeny and regulation of matrix metalloproteinase  
346 activity in the zebrafish embryo by in vitro and in vivo zymography. *Dev. Biol.* *286*, 405–414.
- 347 Ellett, F., Pase, L., Hayman, J.W., Andrianopoulos, A., and Lieschke, G.J. (2011). Mpeg1  
348 Promoter Transgenes Direct Macrophage-Lineage Expression in Zebrafish. *Blood* *117*, e49–e56.
- 349 Friedl, P., and Weigelin, B. (2008). Interstitial leukocyte migration and immune function. *Nat.*  
350 *Immunol.* *9*, 960–969.
- 351 Gering, M., and Patient, R. (2005). Hedgehog signaling is required for adult blood stem cell  
352 formation in zebrafish embryos. *Dev. Cell* *8*, 389–400.
- 353 Gordon, S., and Taylor, P.R. (2005). Monocyte and macrophage heterogeneity. *Nat. Rev.*  
354 *Immunol.* *5*, 953–964.
- 355 Herbomel, P., Thisse, B., and Thisse, C. (1999). Ontogeny and behaviour of early macrophages  
356 in the zebrafish embryo. *Development* *126*, 3735–3745.
- 357 Kimmel, C.B., Ballard, W.W., Kimmel, S.R., Ullmann, B., and Schilling, T.F. (1995). Stages of  
358 embryonic development of the zebrafish. *Dev. Dyn.* *203*, 253–310.
- 359 Kissa, K., and Herbomel, P. (2010). Blood stem cells emerge from aortic endothelium by a novel  
360 type of cell transition. *Nature* *464*, 112–115.
- 361 McWhorter, F.Y., Wang, T., Nguyen, P., Chung, T., and Liu, W.F. (2013). Modulation of  
362 macrophage phenotype by cell shape. *Proc. Natl. Acad. Sci. U. S. A.* *110*, 17253–17258.
- 363 Metchnikoff, É. (1892). Leçons sur la pathologie comparée de l' inflammation : faites à l'  
364 Institut Pasteur en avril et mai 1891 / par Élie Metchnikoff (Paris: Librairie de l'académie de  
365 médecine, 120, Boulevard Saint-Germain, Paris).
- 366 Murayama, E., Kissa, K., Zapata, A., Mordelet, E., Briolat, V., Lin, H.-F., Handin, R.I., and

367 Herbolmel, P. (2006). Tracing hematopoietic precursor migration to successive hematopoietic  
368 organs during zebrafish development. *Immunity* 25, 963–975.

369 Panni, R.Z., Linehan, D.C., and DeNardo, D.G. (2013). Targeting tumor-infiltrating macrophages  
370 to combat cancer. *Immunotherapy* 5, 1075–1087.

371 Sanz-Moreno, V., and Marshall, C.J. (2010). The plasticity of cytoskeletal dynamics underlying  
372 neoplastic cell migration. *Curr. Opin. Cell Biol.* 22, 690–696.

373 Travnickova, J., Tran Chau, V., Julien, E., Mateos-Langerak, J., Gonzalez, C., Lelièvre, E.,  
374 Lutfalla, G., Taviani, M., and Kissa, K. (2015). Primitive macrophages control HSPC  
375 mobilization and definitive haematopoiesis. *Nat. Commun.* 6, 6227.

376 Turk, B. (2006). Targeting proteases: successes, failures and future prospects. *Nat. Rev. Drug*  
377 *Discov.* 5, 785–799.

378 Vérollet, C., Charrière, G.M., Labrousse, A., Cougoule, C., Le Cabec, V., and Maridonneau-  
379 Parini, I. (2011). Extracellular proteolysis in macrophage migration: losing grip for a  
380 breakthrough. *Eur. J. Immunol.* 41, 2805–2813.

381 Westerfield, M. (2000). *The Zebrafish book. A guide for the laboratory use of zebrafish (Danio*  
382 *rerio)*, 4th edition (Eugene).

383 Wheeler, A.P., Wells, C.M., Smith, S.D., Vega, F.M., Henderson, R.B., Tybulewicz, V.L., and  
384 Ridley, A.J. (2006). Rac1 and Rac2 regulate macrophage morphology but are not essential for  
385 migration. *J. Cell Sci.* 119, 2749–2757.

386 Wynn, T. a, Chawla, A., and Pollard, J.W. (2013). Macrophage biology in development,  
387 homeostasis and disease. *Nature* 496, 445–455.

388

389

## 390 **Figure Legends**

391 **Figure 1:** Macrophages in the AGM can be divided into 4 morphological subgroups.

392 (A) The drawing shows a 3D view of vessels and macrophages (red) imaged in B. (B) 3D view of  
393 the AGM in the mid-trunk region of a *Tg(kdrl:eGFP//mpeg1:mCherry-F)* zebrafish embryo at 48  
394 hpf showing the position of vessels (endothelium in green) and macrophages (in red, white  
395 arrows) in the outer side of the vein and in between the dorsal aorta and the cardinal vein. (C)  
396 Diagram of the 4 categories of macrophages delineated according to shape attributes– circularity,  
397 roundness and elongation factor. (D) Representative confocal images (maximum intensity  
398 projections) of individual categories with an outline drawing from particle analysis on the right.  
399 (E) Graph representing the percentage distribution of the different shape categories per AGM.  
400 Data are represented as percentage average  $\pm$  s.e.m. N= 20 embryos. C, caudal; D, dorsal; DA,  
401 dorsal aorta; PCV, posterior cardinal vein; R, rostral; V, ventral. See also supplementary table 1.

402

403 **Figure 2:** Macrophages in the AGM migrate in the mesenchymal way and undergo dynamic  
404 transition between different shapes over time.

405 (A-F) Selected images from Video 1 illustrate the macrophage migration and shape  
406 transformation over time. Numbers point to individual macrophages. Time code is expressed in  
407 hours and minutes. White outlines on panel B-F indicate the shape and position of macrophages  
408 from panel A (9<sup>th</sup> minute). (G-H) Rose plot diagrams show the directionality of macrophage  
409 migration in the AGM compared to the oriented migration of macrophages in the tail region after  
410 tail fin cut injury. A diagram represents the single counts of the position of each macrophage in  
411 the selected area (black and grey sectors of angle  $\pi/18$ ) every minute over 60 minutes with a (x,y  
412 0,0) starting point. n= 23 macrophages for the control and n=27 for directed migration. (I) Graph

413 showing the shape evolution of individual macrophages during a 30 minutes course with 5  
414 minutes interval measurements. Every line represents a single macrophage (n= 10). See also  
415 Video 1. Scale bar, (A-F) 30  $\mu$ m.

416

417 **Figure 3:** Rac inhibition leads to a loss of macrophage plasticity and motility.

418 (A) Graph comparing macrophage shape distribution in the AGM of NSC23766 Rac-inhibited  
419 embryos (Rac Inh) to DMSO treated embryos (control) shows no significant change of  
420 distribution. N=10 embryos for control and 15 for Rac inh. Data are represented as the mean of  
421 the percentage of each shape type in the total macrophage population in the AGM  $\pm$  s.e.m. NS =  
422 not significant. (B-E) Selected cropped images from Video 2 showing the shape and migration of  
423 macrophages over time. Time code in hours and minutes. White outlines on panel C-E indicate  
424 the shape and position of macrophages from panel B (21<sup>st</sup> minute) (F) Graph showing the  
425 velocity of macrophages in control and Rac-inhibited embryos. Data are represented as a mean  $\pm$   
426 s.e.m., n= 15 macrophages from 4 different embryos, \*\*\*\*p<0.0001. (G-H) Tracking plot  
427 diagram representing the migration path and distance of macrophages in the AGM in control and  
428 Rac-inhibited embryos measured every minute for 60 minutes. Scale in  $\mu$ m, n=15 macrophages  
429 from 4 different embryos. (I) Graph shows the shape evolution of individual macrophages during  
430 a 30 minute course with 5 minutes interval measurements, Control to the left, Rac inhibitor to the  
431 right. Each line represents a single macrophage (n= 7). Statistically significant differences exist in  
432 the number of shapes adopted during a 30 minute measurement course (P=0.003) as well as in the  
433 number of changes between two different shapes (P=0.006). (J) *In vivo* zymography in  
434 *Tg(Mpeg1:mCherry)* embryos at 48 hpf reveals the degradation of inserted gelatin (green dots of  
435 cleavage-revealed FITC) in control embryos and a highly reduced degradation after Rac  
436 inhibition. See also Video 2. Scale bar: 30  $\mu$ m.

437

438 **Figure 4:** MMP-9 inhibition induces a change in macrophage shape and a transition towards an  
439 amoeboid-like migration.

440 (A) Graph compares the macrophage shape distribution in the AGM of MMP-2 and 9 (SB-3CT) -  
441 inhibited embryos (MMP inh) to DMSO treated embryos (control) shows an increase in round  
442 shape and a decrease in star-like and elongated shapes in MMP inh embryos. N=10 embryos for  
443 control and 15 for MMP inh. Data represent the percentage mean for each shape type out of the  
444 total number of macrophages in the AGM  $\pm$  s.e.m. NS = not significant; \* $p < 0.05$ ; \*\*\*\* $p < 0.0001$ .

445 (B-E) Selected cropped images from Video 3 displays macrophage shape and migration patterns  
446 over time. Numbers point to individual macrophages, time code is expressed in hours and  
447 minutes. Grey outlines on panel C-E show the shape and position of macrophages from panel B

448 (3<sup>rd</sup> minute). (F) Graph showing the velocity of macrophages in control and MMP-inhibited  
449 embryos. Data are represented as a mean  $\pm$  s.e.m., n= 17 macrophages for control and 14 for  
450 MMP inhibitor from 4 different embryos, \*\*\*\* $p < 0.0001$ . (G-H) Tracking plot diagram represents

451 the migration path and distance of macrophages in the AGM in control and MMP-inhibited  
452 embryos measured every minute over 60 minutes. Scale in  $\mu\text{m}$ , n=17 macrophages for control  
453 and 14 for MMP inhibitor from 4 different embryos. See also Video 3. Scale bar 30  $\mu\text{m}$ . DA,

454 dorsal aorta; PCV, posterior cardinal vein.

455

456 **Supplementary table 1:** Measured average values ( $\pm$  s.e.m.) of shape descriptors for each shape  
457 subgroup. N = 20 embryos.

458

459 **Video 1:** Macrophage 3D migration in the AGM during haematopoiesis.

460 Representative time-lapse colour-depth projections of *Tg(mpeg1:mCherry)* embryo at 46 hpf

461 illustrate macrophages migration occurring in a non-directional manner and through different  
462 depth by appropriately changing colour . Image stacks were acquired every minute over 60  
463 minutes at a 1  $\mu\text{m}$  interval with 1024x256 pixel resolution using the LSM510 Zeiss confocal  
464 microscope equipped with a 40x water immersion objective. Scale bar 30  $\mu\text{m}$ , time code in hours  
465 and minutes.

466

467 **Video 2:** The migratory behaviour of macrophage changes after Rac inhibition.

468 Combined representative time-lapse colour-depth projections of *Tg(mpeg1:mCherry)* embryos at  
469 46 hpf draws a comparison between macrophage migration in DMSO-treated (control, top)  
470 embryos and that of Rac-inhibitor (Rac inh, bottom) treated embryos. Rac-inhibited macrophages  
471 display slower migration modes. They change shapes and migration direction less often, and form  
472 very long membrane extensions. Image stacks were acquired every minute over 60 minutes at a 1  
473  $\mu\text{m}$  interval with 1024x256 pixel resolution using the LSM510 Zeiss confocal microscope  
474 equipped with a 40x water immersion objective. Scale bar 30  $\mu\text{m}$ , time code in hours and minutes.

475

476 **Video 3:** MMP inhibition induces mesenchymal-amoeboid transition of macrophage migration.

477 Combined representative time-lapse colour-depth projections of *Tg(mpeg1:mCherry)* embryos at  
478 46 hpf draw a comparison between macrophage migration in DMSO-treated (control, top) and  
479 MMP-2 and 9 inhibitor (MMP inh, bottom) treated embryos. MMP-inhibited macrophages  
480 migrate faster, adopt a round shape, change the depth of their displacement less often and migrate  
481 partially inside the bloodstream. Image stacks were acquired every minute over 60 minutes at 1  
482  $\mu\text{m}$  interval with 1024x256 pixel resolution using the LSM510 Zeiss confocal microscope  
483 equipped with a 40x water immersion objective. Scale bar 30  $\mu\text{m}$ , time code expressed in hours  
484 and minutes.

Figure 1

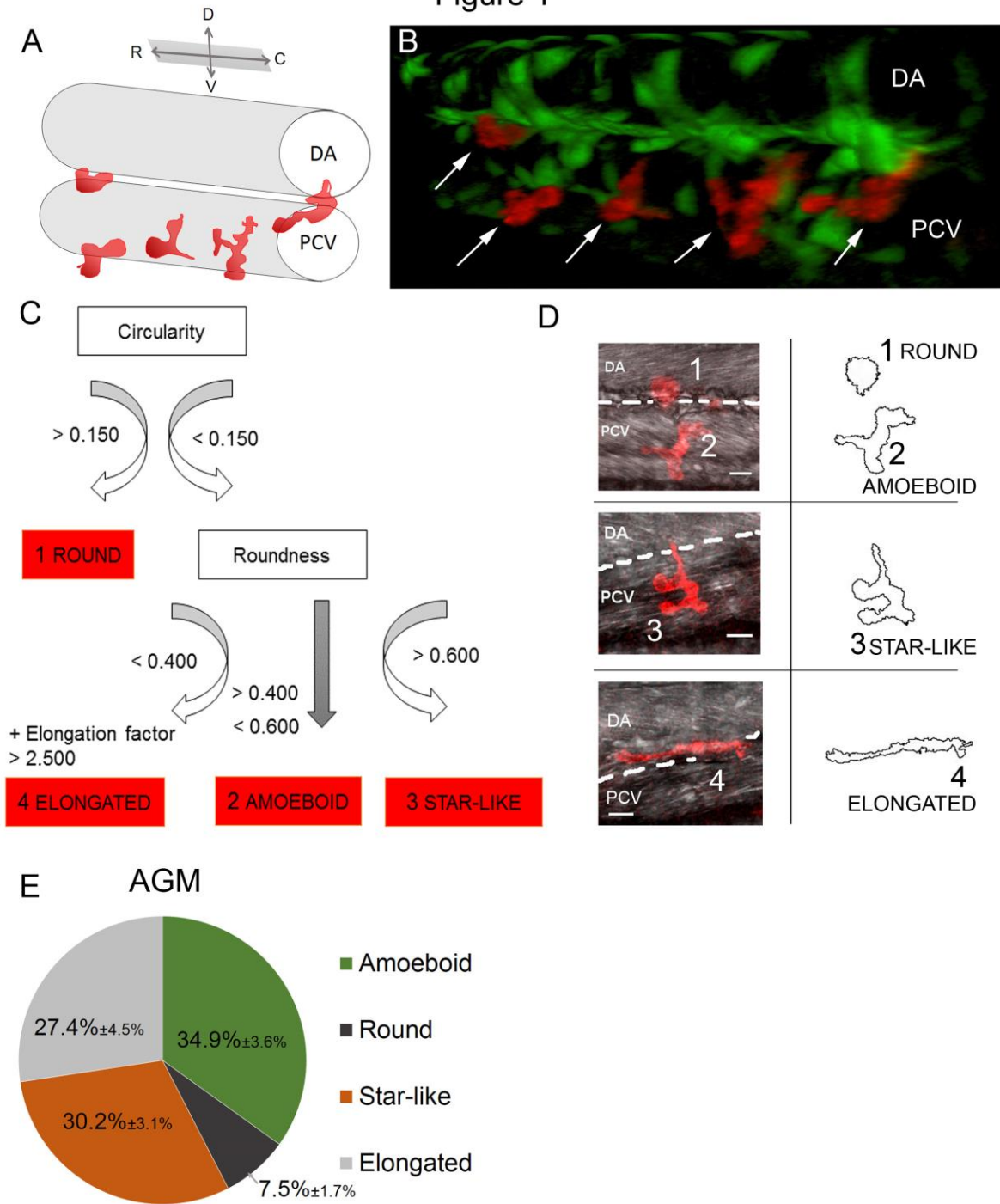


Figure 2

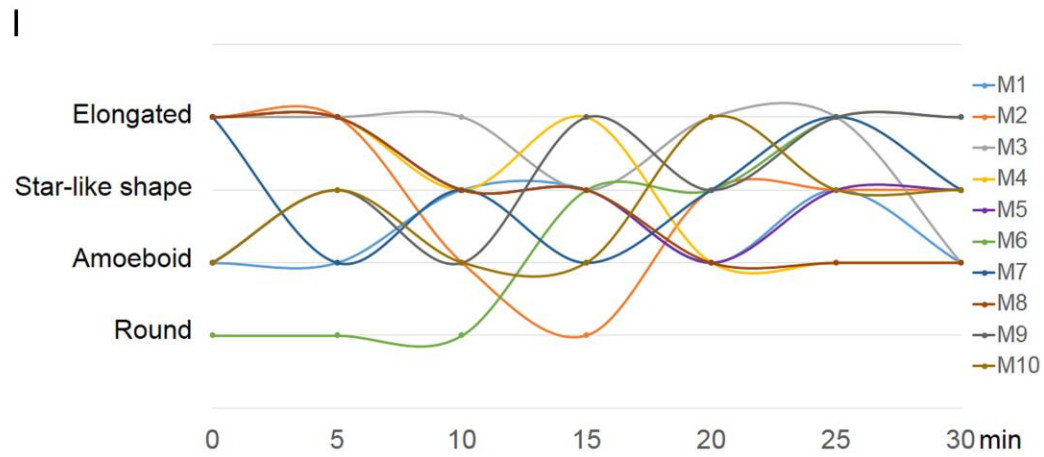
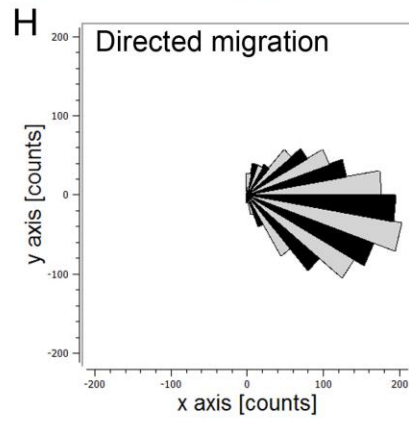
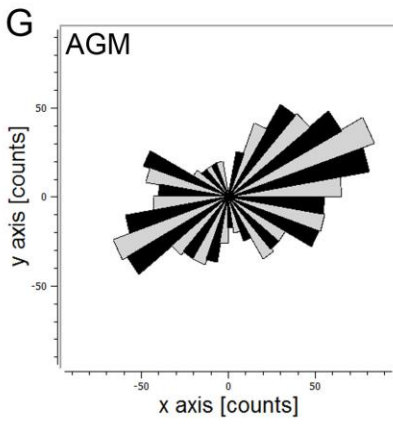
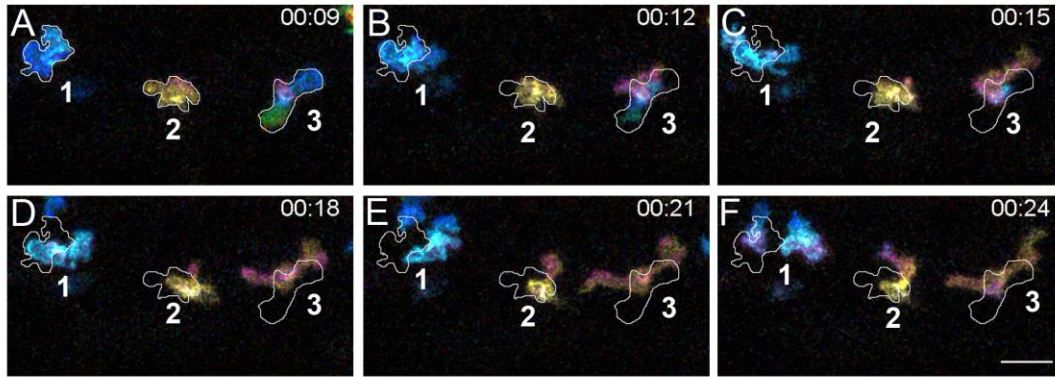


Figure 3

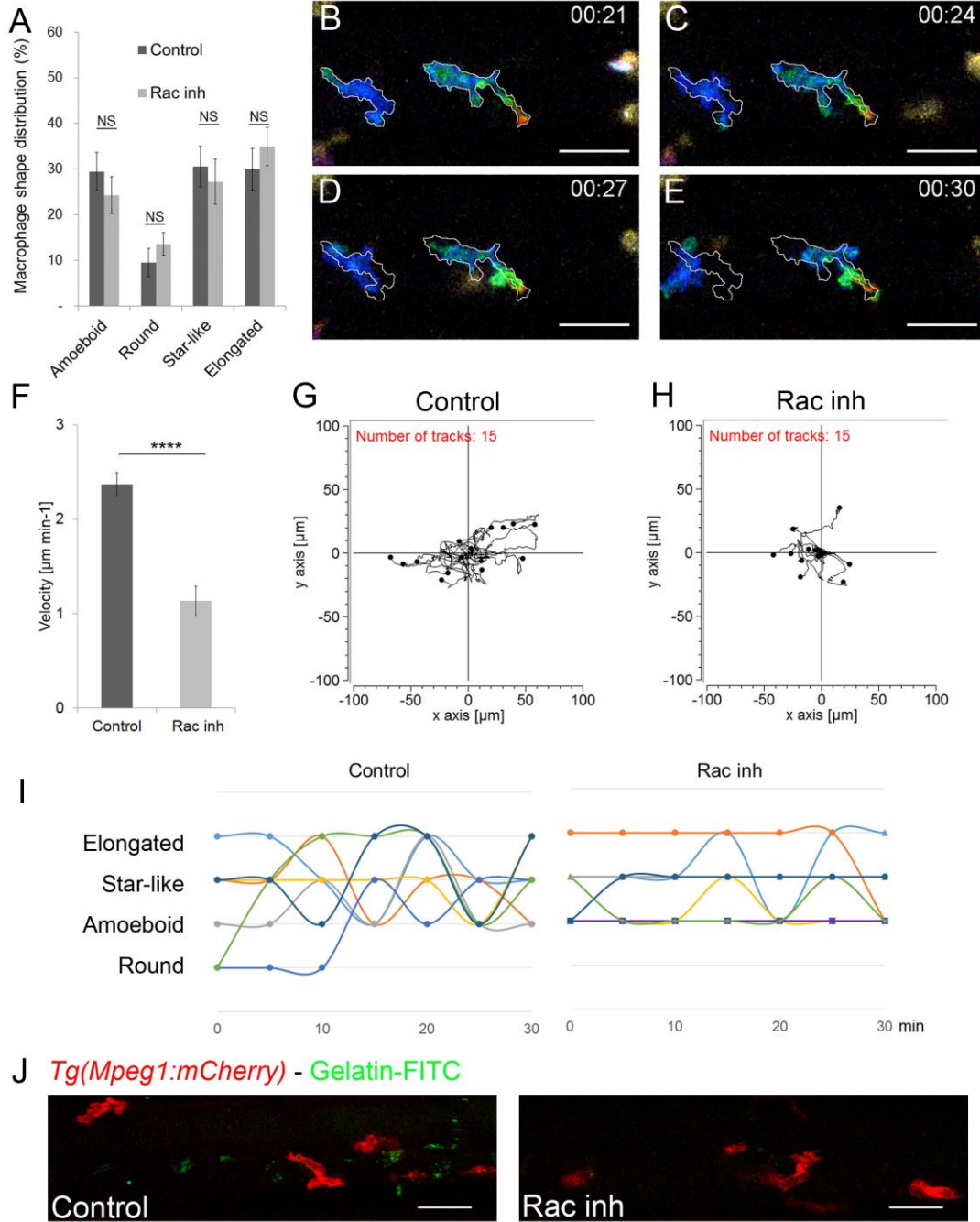
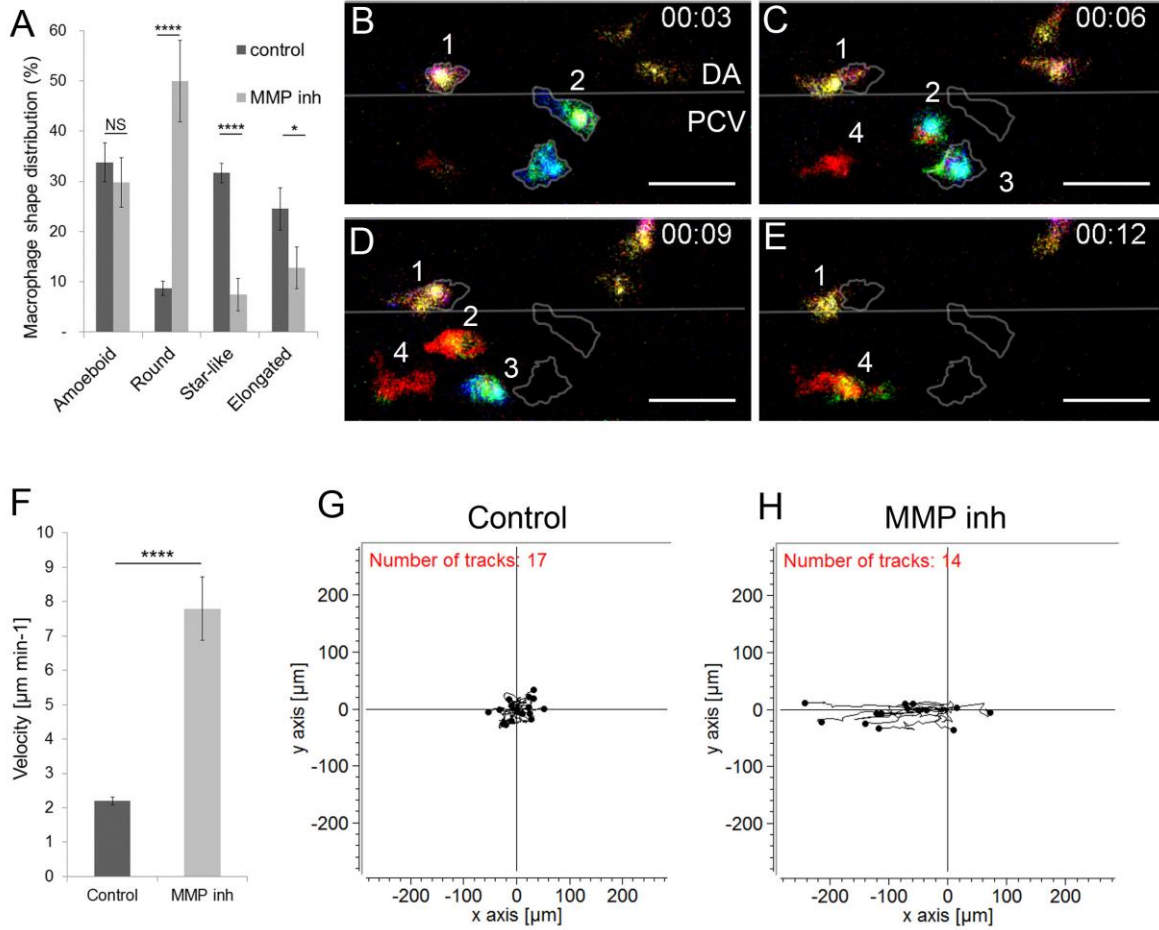


Figure 4



# Figures

Figure 1

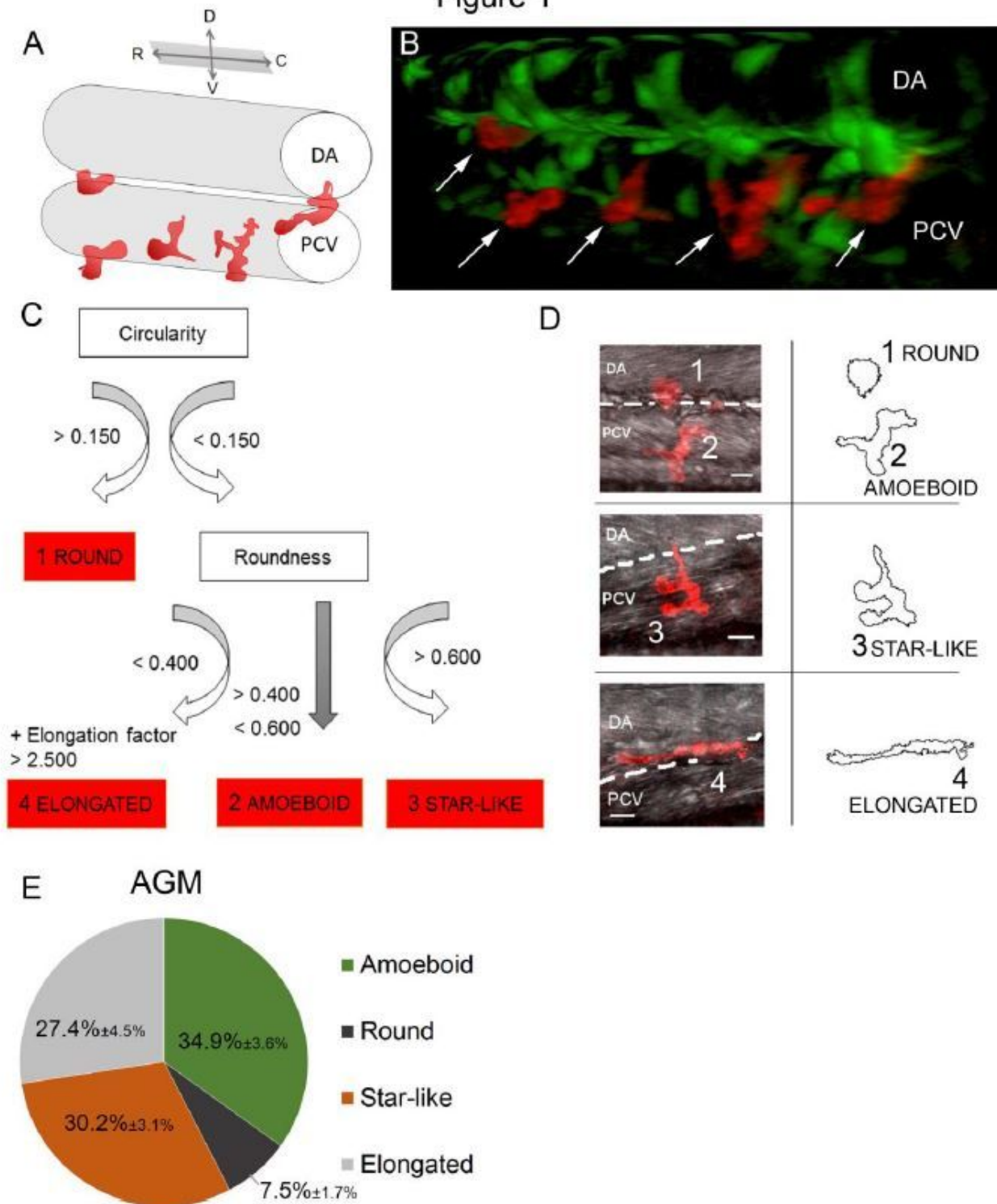
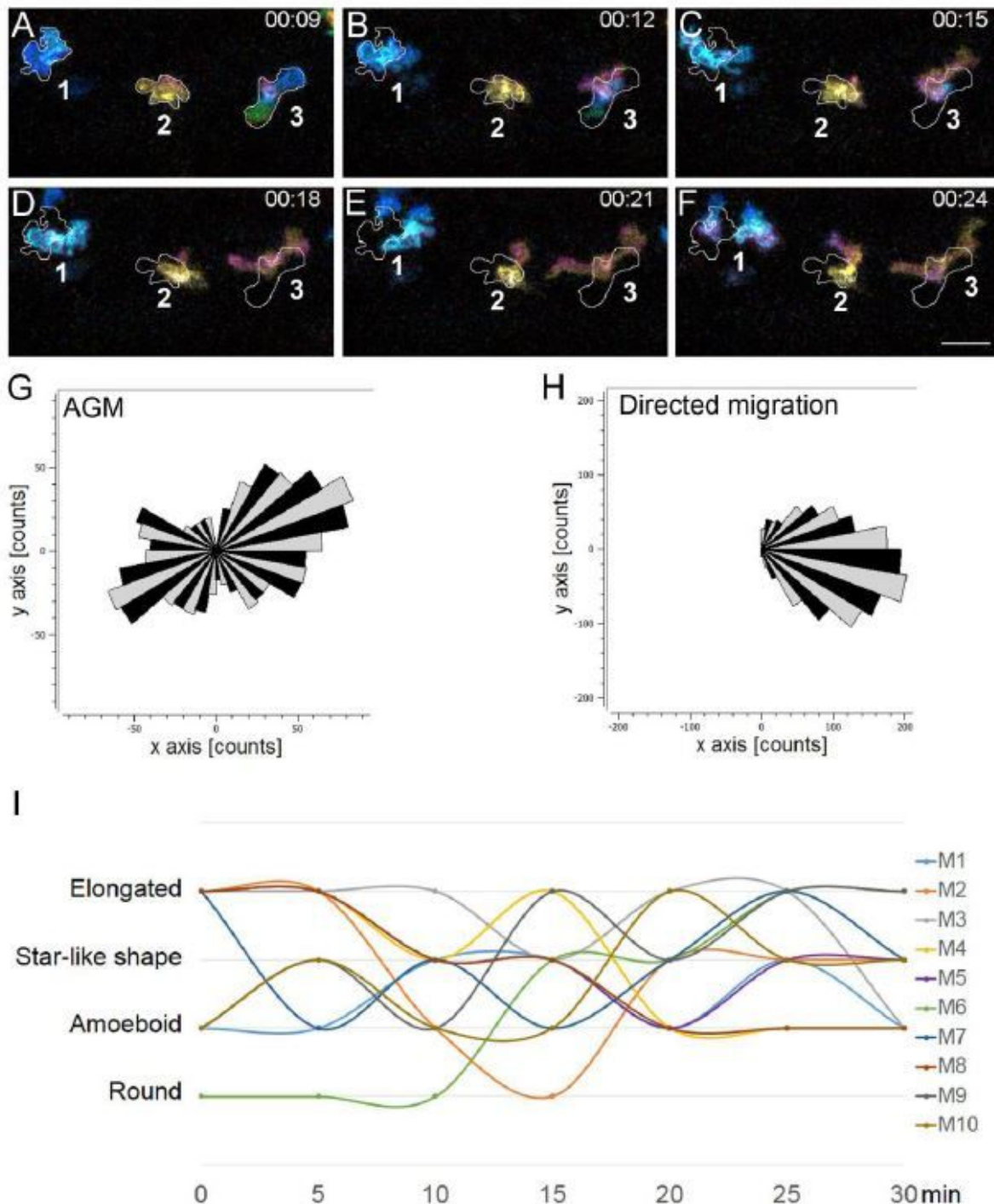


Figure 1

Macrophages in the AGM can be divided into 4 morphological subgroups. (A) The drawing shows a 3D view of vessels and macrophages (red) imaged in B. (B) 3D view of the AGM in the mid-trunk region of a *Tg(kdrl:eGFP//mpeg1:mCherry-F)* zebrafish embryo at 48 hpf showing the position of vessels

(endothelium in green) and macrophages (in red, white arrows) in the outer side of the vein and in between the dorsal aorta and the cardinal vein. (C) Diagram of the 4 categories of macrophages delineated according to shape attributes– circularity, roundness and elongation factor. (D) Representative confocal images (maximum intensity projections) of individual categories with an outline drawing from particle analysis on the right. (E) Graph representing the percentage distribution of the different shape categories per AGM. Data are represented as percentage average  $\pm$  s.e.m. N= 20 embryos. C, caudal; D, dorsal; DA, dorsal aorta; PCV, posterior cardinal vein; R, rostral; V, ventral. See also supplementary table 1.

Figure 2



## Figure 2

Macrophages in the AGM migrate in the mesenchymal way and undergo dynamic transition between different shapes over time. (A-F) Selected images from Video 1 illustrate the macrophage migration and shape transformation over time. Numbers point to individual macrophages. Time code is expressed in hours and minutes. White outlines on panel B-F indicate the shape and position of macrophages from panel A (9th minute). (G-H) Rose plot diagrams show the directionality of macrophage migration in the AGM compared to the oriented migration of macrophages in the tail region after tail fin cut injury. A diagram represents the single counts of the position of each macrophage in the selected area (black and grey sectors of angle  $\pi/18$ ) every minute over 60 minutes with a (x,y 0,0) starting point. n= 23 macrophages for the control and n=27 for directed migration. (I) Graph showing the shape evolution of individual macrophages during a 30 minutes course with 5 minutes interval measurements. Every line represents a single macrophage (n= 10). See also Video 1. Scale bar, (A-F) 30  $\mu\text{m}$ .

### Figure 3

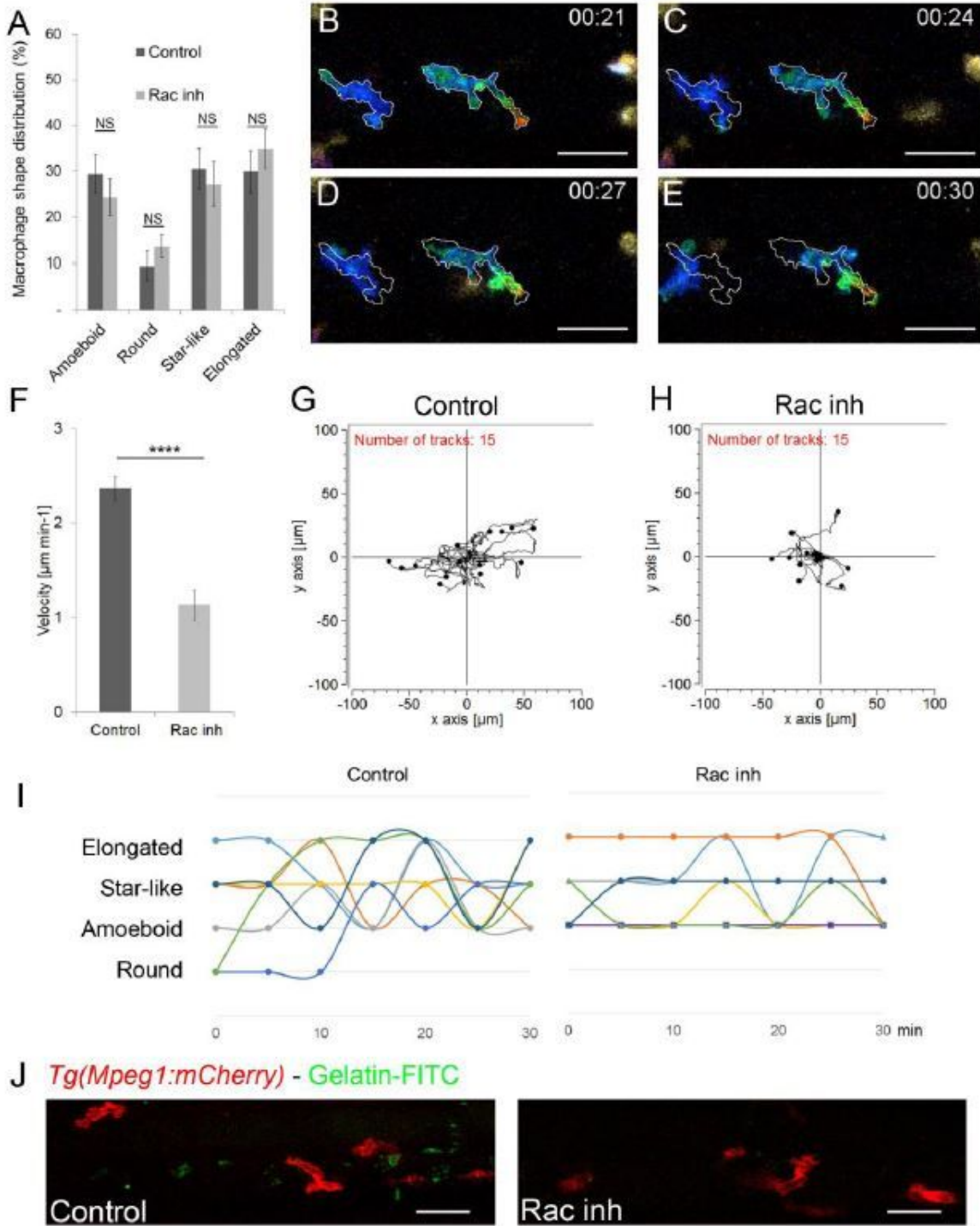


**Figure 3**

Rac inhibition leads to a loss of macrophage plasticity and motility. (A) Graph comparing macrophage shape distribution in the AGM of NSC23766 Rac-inhibited embryos (Rac Inh) to DMSO treated embryos (control) shows no significant change of distribution. N=10 embryos for control and 15 for Rac inh. Data are represented as the mean of the percentage of each shape type in the total macrophage population in the AGM  $\pm$  s.e.m. NS = not significant. (B-E) Selected cropped images from Video 2 showing the shape

and migration of macrophages over time. Time code in hours and minutes. White outlines on panel C-E indicate the shape and position of macrophages from panel B (21st minute) (F) Graph showing the velocity of macrophages in control and Rac-inhibited embryos. Data are represented as a mean  $\pm$  s.e.m.,  $n = 15$  macrophages from 4 different embryos, \*\*\*\* $p < 0.0001$ . (G-H) Tracking plot diagram representing the migration path and distance of macrophages in the AGM in control and Rac-inhibited embryos measured every minute for 60 minutes. Scale in  $\mu\text{m}$ ,  $n = 15$  macrophages from 4 different embryos. (I) Graph shows the shape evolution of individual macrophages during a 30 minute course with 5 minutes interval measurements, Control to the left, Rac inhibitor to the right. Each line represents a single macrophage ( $n = 7$ ). Statistically significant differences exist in the number of shapes adopted during a 30 minute measurement course ( $P = 0.003$ ) as well as in the number of changes between two different shapes ( $P = 0.006$ ). (J) In vivo zymography in Tg(Mpeg1:mCherry) embryos at 48 hpf reveals the degradation of inserted gelatin (green dots of cleavage-revealed FITC) in control embryos and a highly reduced degradation after Rac inhibition. See also Video 2. Scale bar:  $30 \mu\text{m}$ .

Figure 4

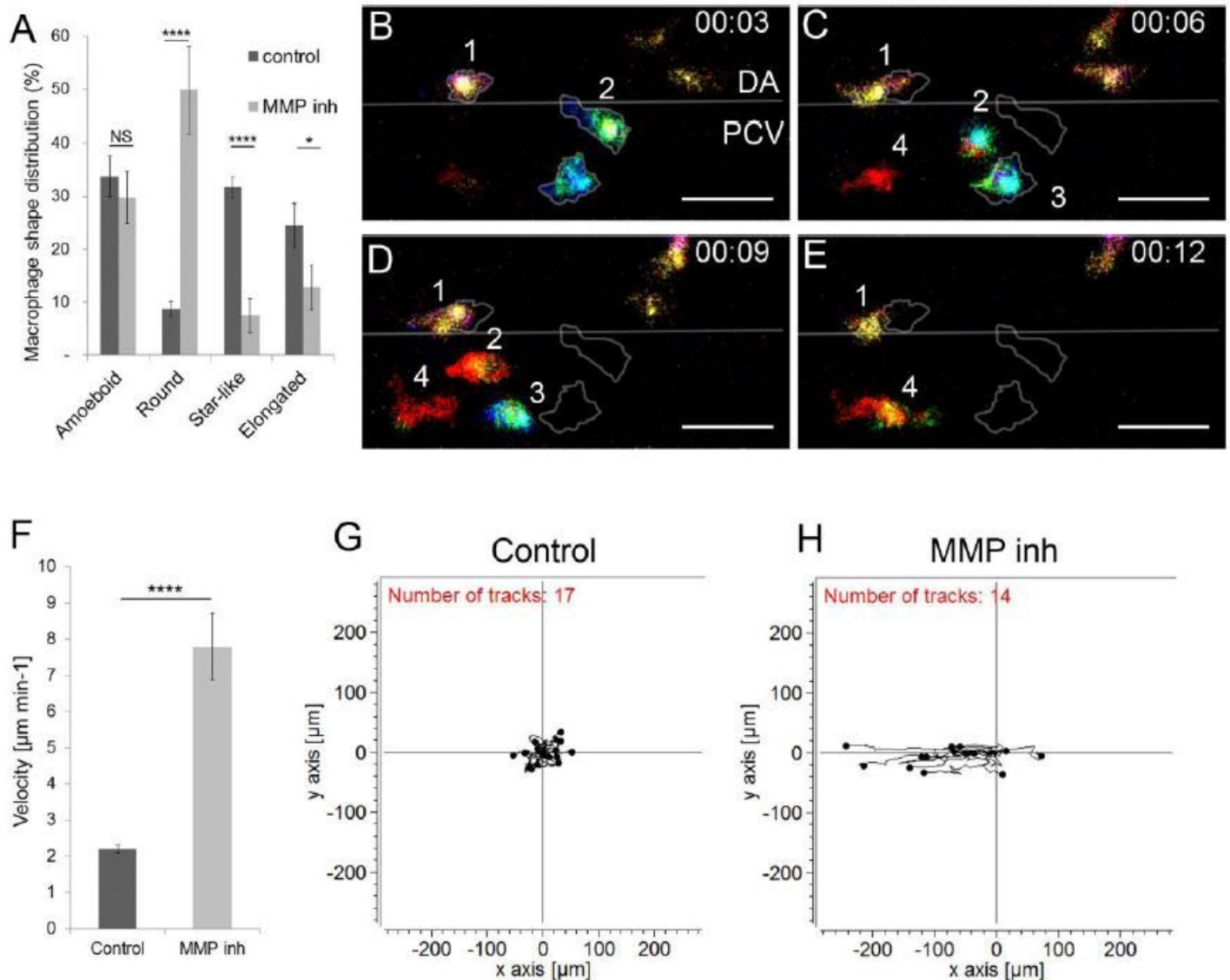


## Figure 4

MMP-9 inhibition induces a change in macrophage shape and a transition towards an amoeboid-like migration. (A) Graph compares the macrophage shape distribution in the AGM of MMP-2 and 9 (SB-3CT)-inhibited embryos (MMP inh) to DMSO treated embryos (control) shows an increase in round shape and a decrease in star-like and elongated shapes in MMP inh embryos. N=10 embryos for control and 15 for MMP inh. Data represent the percentage mean for each shape type out of the total number of macrophages in the AGM  $\pm$  s.e.m. NS = not significant; \* $p < 0.05$ ; \*\*\*\* $p < 0.0001$ . (B-E) Selected cropped images from Video 3 displays macrophage shape and migration patterns over time. Numbers point to individual macrophages, time code is expressed in hours and minutes. Grey outlines on panel C-E show the shape and position of macrophages from panel B (3rd minute). (F) Graph showing the velocity of macrophages in control and MMP-inhibited embryos. Data are represented as a mean  $\pm$  s.e.m., n= 17 macrophages for control and 14 for MMP inhibitor from 4 different embryos, \*\*\*\* $p < 0.0001$ . (G-H) Tracking plot diagram represents the migration path and distance of macrophages in the AGM in control and MMP-inhibited embryos measured every minute over 60 minutes. Scale in  $\mu\text{m}$ , n=17 macrophages for control and 14 for MMP inhibitor from 4 different embryos. See also Video 3. Scale bar 30  $\mu\text{m}$ . DA, dorsal aorta; PCV, posterior cardinal vein.

## Supplementary Files

This is a list of supplementary files associated with this preprint. Click to download.

- [SuppTable1TravnickovaetalScientificReport14nov2020.pdf](#)
- [Video1TravnickovaetalScientificReport14nov2020.avi](#)
- [Video2TravnickovaetalScientificReport14nov2020.avi](#)
- [Video3TravnickovaetalScientificReport14nov2020.avi](#)